Journal of Computational Acoustics Vol. 1, No. 1 (1993) 117–140

THEORY OF ACOUSTIC IMAGING IN THE OCEAN WITH AMBIENT NOISE

MICHAEL J. BUCKINGHAM
Marine Physical Laboratory, Scripps Institution of Oceanography
La Jolla, California 92093, USA
and
Institute of Sound and Vibration Research
The University, Southampton, SO9 5NH, England

Received 21 October 1992
Revised 13 November 1992

Following a recent experiment in which ambient noise (acoustic daylight) was used as the sole source of acoustic illumination for detecting objects in the ocean, a full wave-theoretic analysis is presented in this article of the visibility of a pressure-release spherical target when illuminated by ambient noise showing various degrees of anisotropy. The basis of the analysis is a new, accurate approximation for the Green's function representing the field around the sphere. From this expression, an analysis of the acoustic contrast is developed, as observed at the output of an endfire line array, which constitutes the acoustic lens. Our essential conclusion is that, even in isotropic noise, which presents one of the least favourable conditions for incoherent imaging, the visibility of the sphere (i.e. the ratio of intensities with the sphere present and absent) is approximately 4 dB. This is consistent with our early experimental observations, and is adequate to form the basis of an acoustic daylight imaging system.

1. Introduction

The concept of imaging objects in the ocean using ambient noise as the sole source of acoustic "illumination" was proposed several years ago.[3] In several respects, the new technique is analogous to the way in which photographic or video images are formed using ambient light (daylight) in the atmosphere. Essentially, a photographic image is a pictorial record of the optical intensity contrast between elements of differing reflectivity in the object space. Imaging techniques, such as conventional photography, which depend on intensity rather than phase, are henceforth referred to as "incoherent" techniques. (Such techniques are distinct from coherent imaging, exemplified by holography, where the phase of the field is crucially important to the image formation process.)

Ambient noise in the ocean has much in common with daylight in the atmosphere. In both cases, the radiation field consists of energy propagating with random phases in all directions, suggesting that ambient noise may be thought of as the "acoustic daylight" of

the ocean. Since daylight is the basis of photography in the atmosphere, it is natural by analogy to speculate on the possibility of using ambient noise for incoherent imaging of objects beneath the sea surface.

Any object present in the oceanic noise field modifies the field by acting as a scattering agent. By focusing the scattered radiation using an appropriate acoustic lens (which could be a reflector, refractor or phased array), a pictorial image of the object space will be formed on the focal surface. The image of the object itself should be distinguishable against the image of the background through the intensity contrast that arises from the object's acoustic albedo.

To test the idea of incoherent imaging with acoustic daylight, an experiment was conducted recently off Scripps pier in which a parabolic reflector (the acoustic lens) with a single hydrophone at the focus was used to detect submerged rectangular targets that were illuminated solely by naturally generated ambient noise.[5] With such a rudimentary lens, it was impossible to form a recognizable image of the targets since the parabolic dish showed only one "look" direction, corresponding to just a single pixel on a video monitor. However, by looking for a change in the level of the received signal when a target was placed in the beam, it was possible to establish whether intensity differences across the object space were detectable.

The experiment was successful. In effect, the targets were "seen" over a noise frequency band between 5 and 50 kHz. Across the band, the spectral level was higher by a nominal 4 dB when the targets were present in the beam of the reflector, compared with when they were absent. This observation was repeated continuously over a period of several days, and then again after about three months, when the whole system was re-assembled and deployed for a further period of several days. For logistical reasons, it was not possible to monitor the horizontal structure of the noise field during these experiments, but circumstantial evidence suggests that the pier itself may have been a source of noise, in which case the configuration of parabolic dish and targets was akin to taking a photograph with the sun behind the camera (front illumination).

The question of how the degree of anisotropy of the ambient noise field affects the "contrast" ratio at the output of the receiver (i.e. the ratio of the output power with a target present to that with target absent) is fundamental to the operation of the acoustic daylight system. Isotropy of the noise, at least in the horizontal, must be regarded as an important operating condition, since it is representative of many oceanic environments; but various degrees of anisotropy may also be expected, associated for example with the direction in which the sea surface waves are propagating.[12] Image formation with isotropic noise is roughly equivalent to photography in the atmosphere on an overcast day, and is by no means unworkable. Any anisotropy will tend to modify the acoustic contrast, the effect being usually to improve the quality of the image. Back-illumination, for example, produces a shadow in the field, that is to say the target is visible as a silhouette. Conventional, front-illumination also produces good acoustic contrast, with the target bright against a darker background.

To quantify the contrast ratio (or acoustic contrast) under various degrees of anisotropy in the noise field, an analysis of incoherent acoustic imaging of a spherical target is developed in this article. Rather than a parabolic reflector, we consider as the acoustic lens a phased array of equi-distant collinear hydrophones steered to endfire. The theoretical argument proceeds by first establishing the Green's function of the field from a point source in the presence of the spherical scatterer, and then extending this deterministic result to give the spatial statistics of the field from a distribution of independent noise sources located on a large spherical surface concentric with the scattering object. By this technique, when the radius of the large source sphere is allowed to go to infinity, we generate a plane-wave (i.e. spatially homogeneous) noise field whose anisotropy is governed by the angular distribution of the noise sources on the large sphere, and superimposed upon this incident field is the (spatially inhomogeneous) noise component scattered from the target sphere.

As shown below, the expressions for the acoustic power of the scattered and incident components of the noise field separate into two additive terms, making it a straightforward matter to formulate the contrast ratio as measured at the output of the acoustic lens. For convenience, we define the acoustic visibility as the contrast expressed in dB. Naturally, the visibility depends on the radius (in wavelengths) of the scattering object, the aperture of the acoustic lens, the distance (in wavelengths) of the lens from the spherical target, and the angular distribution of the noise sources on the large source sphere. With this fairly general result, we are able to estimate the performance of an acoustic daylight imaging system in a variety of ambient noise conditions. Taking as an example the case of isotropic noise, we find that the visibility shows a maximum value of approximately 4 dB, occurring when the angle of view of the acoustic lens matches the angle subtended by the target at the phase centre of the array. This level of visibility is consistent with our observations made in the recent experiment conducted off Scripps pier, and should be adequate for providing distinguishable, pictorial images using the acoustic daylight technique.

2. The Green's Function

To begin, consider a spherical pressure-release target which is irradiated by a point impulsive source, the objective being to determine the field surrounding the target. When the source is at infinite distance from the sphere (i.e. the incident field consists of plane waves), this problem has a well-known solution (see e.g. [10]). We are initially interested in the more general case in which the source is at finite range (Fig. 1). Spherical polar coordinates are the natural choice for the problem, with the origin at the centre of the target sphere and the axis passing through the source. From symmetry, the field is independent of the azimuthal angle, ϕ, but depends on the ranges r and r' of the receiver and source, respectively, the polar angle of the receiver, θ, and the radius of the sphere, b.

Since we are interested in the spectral response of the acoustic daylight system, we require the Fourier transform (with respect to time) of the Green's function, G. This is given by the solution of the Helmholtz equation which, in spherical coordinates, is

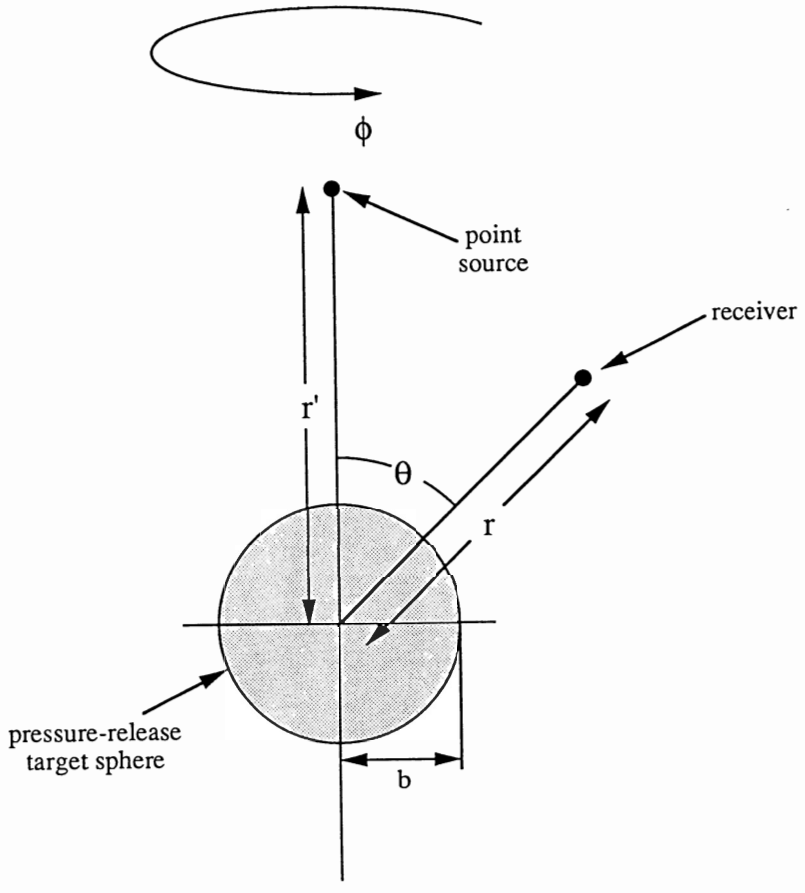

Fig. 1. Geometry for the problem of scattering by a spherical object. The point source is at radius r' and the receiver at radius r, measured from the centre of the target sphere of radius b.

$$\frac{1}{r^2}\frac{\partial}{\partial r}\left(r^2\frac{\partial G}{\partial r}\right)+\frac{1}{r^2\sin\theta}\frac{\partial}{\partial\theta}\left(\sin\theta\frac{\partial G}{\partial\theta}\right)+k^2G=-Q\frac{\delta(r-r')\delta(\theta)}{2\pi r^2\sin\theta}, \tag{1}$$

where δ is the Dirac delta function, k is the acoustic wavenumber and Q is the source strength. By making the substitution

$$G=\frac{w}{r^{1/2}}, \tag{2}$$

where w is a new field variable, the Helmholtz equation becomes

$$\frac{\partial^2 w}{\partial r^2}+\frac{1}{r}\frac{\partial w}{\partial r}+\frac{1}{r^2}\left\{\frac{1}{\sin\theta}\frac{\partial}{\partial\theta}\left(\sin\theta\frac{\partial w}{\partial\theta}\right)-\frac{w}{4}\right\}+k^2w=-Q\frac{\delta(r-r')\delta(\theta)}{2\pi r^{3/2}\sin\theta}, \tag{3}$$

which is to be solved subject to the boundary condition

$$w=0 \quad \text{at} \quad r=b, \tag{4}$$

and the requirement that the radiation condition be satisfied.

The solution of Eq. (3) is obtained by applying sequentially two integral transforms, a Legendre transform over the polar angle, θ, and a Hankel transform over the range, r. This yields an algebraic expression for the doubly transformed field, from which the field itself is obtained by the application of the corresponding inverse transforms. A similar procedure has been discussed by Buckingham[4] and so the details are not repeated here. The result for the field G is

$$G \equiv G(r, b) = j\frac{Q}{4\sqrt{rr'}} \sum_{n=0}^{\infty} \left(n + \frac{1}{2}\right) \{g_n(r) - f_n(r, b)\} P_n(\cos\theta), \tag{5}$$

where $j = \sqrt{-1}$, $P_n(\cos\theta)$ is the Legendre function of order n, and

$$g_n(r) = H_\nu^{(1)}(kr')J_\nu(kr), \tag{6a}$$

$$f_n(r, b) = \frac{H_\nu^{(1)}(kr')J_\nu(kb)H_\nu^{(1)}(kr)}{H_\nu^{(1)}(kb)}. \tag{6b}$$

In Eqs. (6), J_ν and $H_\nu^{(1)}$ are, respectively, the Bessel function of the first kind and the Hankel function of the first kind, both of order $\nu = (n + 1/2)$.

The first term, g_n, in parenthesis in Eq. (5) represents the incident field and the second term, f_n, the scattered field. This is obvious, for in the limiting case when $b = 0$, corresponding to the absence of the scattering sphere, the Bessel function $J_\nu(0)$ is zero and thus the component f_n is also zero. It follows that f_n must represent the scattered field. Through the use of a Bessel function addition theorem, the expression for the incident field in Eqs. (5) and (6a) is easily shown to reduce to the more familiar form

$$G(r, 0) = \frac{Qe^{jk\rho}}{4\pi\rho}, \tag{7}$$

where

$$\rho = (r^2 + r'^2 - 2rr'\cos\theta)^{1/2} \tag{8}$$

is the distance between the source and receiver. Equation (7) is the classic result for the field from a point source in an unbounded homogeneous medium.

The separation of the Green's function in Eq. (5) into additive components, one of which represents the incident field and the other the scattered field, is well known. Later, we shall see that this separation of terms leads to a similar separation in the expression for the noise power, which will be useful in formulating the contrast ratio at the output of the acoustic lens.

Before addressing the question of the noise field, it is expedient to examine the Green's function with the intention of deriving an approximate representation of G which is more tractable than the infinite summation in Eq. (5). With this in mind, it is convenient to

anticipate that we shall be assuming all the noise sources are at an infinite range from the scattering sphere. Hence, the Hankel function containing the source range, r', in the argument may be approximated by its asymptotic form:

$$\lim_{kr'\to\infty} H_\nu^{(1)}(kr') = \sqrt{\frac{2}{\pi kr'}} \exp j\left[kr' - \left(\nu + \frac{1}{2}\right)\frac{\pi}{2}\right]. \tag{9}$$

The Green's function in Eq. (5) then reduces to

$$G = \frac{jQ}{4r'}\sqrt{\frac{2}{\pi kr}} \exp(jkr')\{S - T\}, \tag{10}$$

where

$$S = \sum_{n=0}^{\infty} (-j)^{n+1}\left(n + \frac{1}{2}\right) J_\nu(kr)P_n(\cos\theta) \equiv -\frac{j}{2}\sqrt{\frac{2kr}{\pi}} \exp(-jkr\cos\theta) \tag{11}$$

represents the incident field and

$$T = \sum_{n=0}^{\infty} (-j)^{n+1}\left(n + \frac{1}{2}\right) \frac{J_\nu(kb)H_\nu^{(1)}(kr)}{H_\nu^{(1)}(kb)} P_n(\cos\theta) \tag{12}$$

is the scattered field. The identity between the last two expressions in Eq. (11) is the degenerate form of a Bessel function addition theorem.[13]

Although the expression for the incident field, S, in Eq. (11) has reduced to a simple closed form, the infinite summation for the scattered field in Eq. (12) still represents a problem. To evaluate this sum approximately, we concentrate on the two Hankel functions and represent them by the following asymptotic approximation:[1]

$$H_\nu^{(1)}(x) = \sqrt{\frac{2}{\pi x}} \exp j\left[x - \left(\nu + \frac{1}{2}\right)\frac{\pi}{2}\right] \cdot \left\{1 + j\frac{(4\nu^2 - 1)}{1!(8x)} - \frac{(4\nu^2 - 1)(4\nu^2 - 9)}{2!(8x)^2} + \cdots\right\}. \tag{13}$$

Now, the asymptotic series in parenthesis is approximated by an exponential function:

$$1 + j\frac{(4\nu^2 - 1)}{1!(8x)} - \frac{(4\nu^2 - 1)(4\nu^2 - 9)}{2!(8x)^2} + \cdots \approx \exp\left\{j\frac{\nu^2}{2x}\right\}, \tag{14}$$

allowing the Hankel function in Eq. (13) to be expressed as

$$H_\nu^{(1)}(x) \approx \sqrt{\frac{2}{\pi x}} \exp j\left[x - \left(\nu + \frac{1}{2}\right)\frac{\pi}{2} + \frac{\nu^2}{2x}\right]. \tag{15}$$

With the help of this approximation plus a little algebra, the quotient of Hankel functions in Eq. (12) becomes

$$\frac{H_\nu^{(1)}(kr)}{H_\nu^{(1)}(kb)} \approx b\sqrt{\frac{\pi k}{2(r-b)}}\exp\left[jk\left(r-b+\frac{br}{r-b}\right)\right]\exp\left[-j\left(\nu+\frac{1}{2}\right)\frac{\pi}{2}\right]H_\nu^{(2)}\left(\frac{krb}{r-b}\right), \tag{16}$$

where the Hankel function of the second kind, $H_\nu^{(2)}$, appears through the use of the conjugated version of Eq. (15). On substituting Eq. (16) into Eq. (12), the expression for T takes the form

$$T \approx b\sqrt{\frac{\pi k}{2(r-b)}}\exp\left[jk\left(r-b+\frac{br}{r-b}\right)\right] \times \sum_{n=0}^{\infty}(-1)^{n+1}\left(n+\frac{1}{2}\right)J_\nu(kb)H_\nu^{(2)}\left(\frac{krb}{r-b}\right)P_n(\cos\theta). \tag{17}$$

Equation (17) represents considerable progress, since the infinite sum may now be expressed in closed form through a Bessel function addition theorem.[8] The result is

$$T \approx -\frac{kb}{2}\sqrt{\frac{bb'}{(r-b)Z}}\exp[jk(r-b+b')]H_{\frac{1}{2}}^{(2)}(kZ), \tag{18}$$

where

$$b' = \frac{br}{(r-b)}, \tag{19}$$

and

$$Z \equiv Z(\theta) = \sqrt{(b'-b)^2+4bb'\cos^2(\theta/2)}. \tag{20}$$

Since the Hankel function of half-integer order in Eq. (18) can be expressed exactly in terms of an elementary function as follows,

$$H_{\frac{1}{2}}^{(2)}(kZ) = j\sqrt{\frac{2}{\pi kZ}}\exp(-jkZ), \tag{21}$$

the expression for T in Eq. (18) simplifies still further to

$$T \approx -jb\sqrt{\frac{kbb'}{2\pi(r-b)}}\exp[jk(r-b+b')]\frac{\exp(-jkZ)}{Z}. \tag{22}$$

Through Eqs. (11) and (22), the Green's function for the field around the scattering sphere is represented by a closed-form expression involving only elementary functions. The new approximation in Eq. (22) for the scattered component differs from previously known approximations developed, for example, by Morse and Ingard.[11] It is valid for short and

intermediate wavelengths, that is to say, when $kb \geq 1$, and is remarkably accurate over a wide range of the geometrical parameters kr and θ.

Figures 2 and 3 show comparisons between the exact Green's function (Eqs. (10), (11), and (12)) and the new closed form expression for G (Eqs. (10), (11), and (22)). (It should be noted that, in the far-field plots of Figs. 2 and 3, where $kr = 10^3$ or 10^4, only the region in the vicinity of the shadow edge is illustrated, since the curves elsewhere are almost indistinguishable. There is thus a considerable expansion of the abscissae in these plots, which emphasizes the differences between the exact and approximate forms for G). It can be seen that in all cases, near-field and far-field, the approximation is essentially exact when θ is small, that is to say, in the back-scattering regime. This is true for all values of $kb \geq 1$. For values of θ approaching π, corresponding to forward scattering, the approximation remains excellent provided $(r/b) \gg 1$, that is to say, in the far field. Under this condition, the spatial phase and the shadow edge are well represented by the approximation, although the amplitudes of the spatial oscillations show a small error, in the region of a few percent; and the shadow according to the approximation is deeper than the true shadow. As the receiver is moved closer to the scattering sphere, more significant

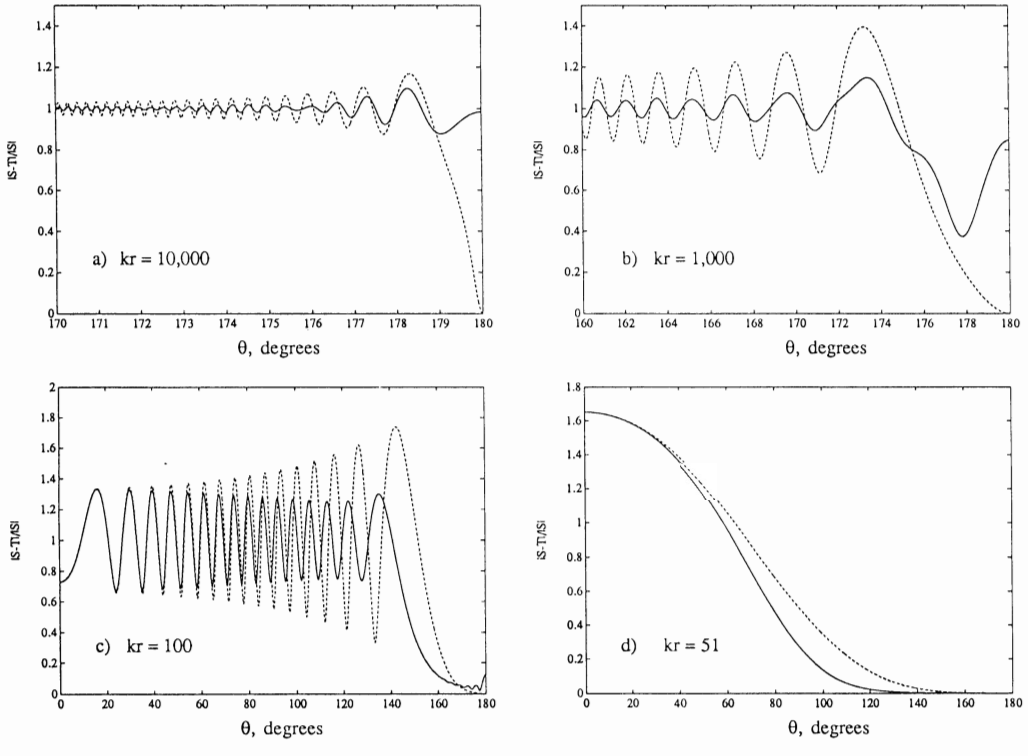

Fig. 2. Plots of the normalized Green's function $|G(r, b)/G(r, 0)| = |S - T|/|S|$ for $kb = 50$. The solid line is the exact expression in Eqs. (10), (11), and (12) and the dashed line is from Eq. (11) for S and Eq. (22) for the approximation to T.

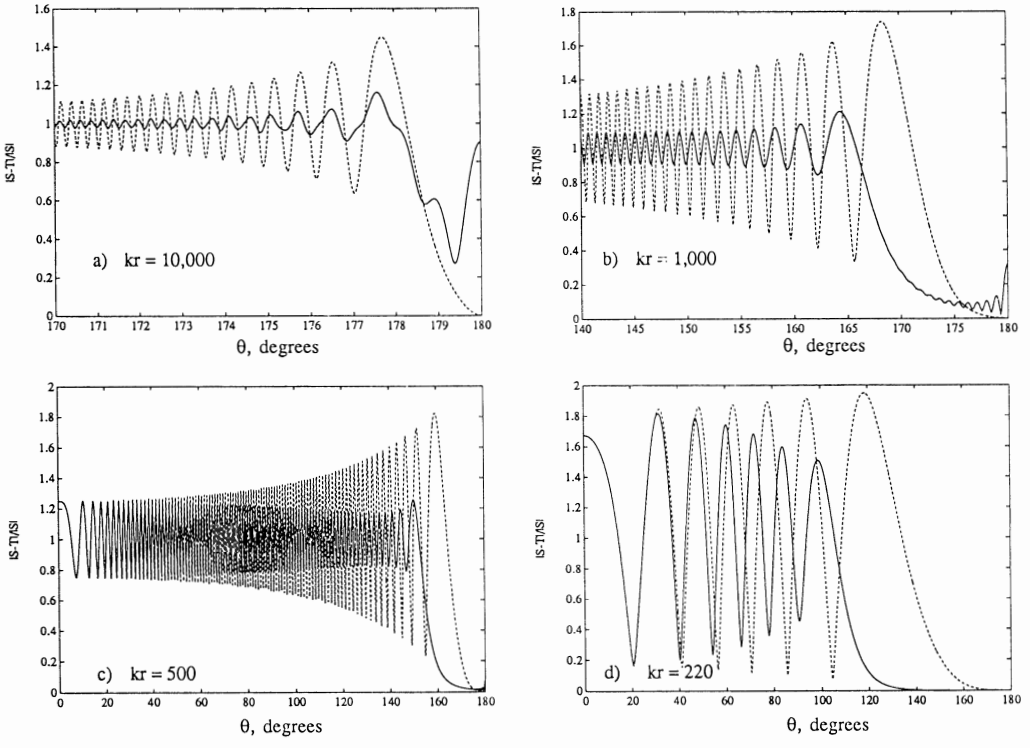

Fig. 3. Plots of the normalized Green's function $|G(r, b)/G(r, 0)| = |S - T|/|S|$ for $kb = 200$. The solid line is the exact expression in Eqs. (10), (11), and (12) and the dashed line is from Eq. (11) for S and Eq. (22) for the approximation to T.

errors begin to appear in the spatial phase, the amplitudes of the spatial oscillations, and the angular position of the shadow edge. These errors, however, are hardly dramatic and in the context of the acoustic daylight analysis which follows, are of little consequence since we shall be concerned primarily with the far field, where the approximation for the scattered field, T, in Eq. (22) is very satisfactory.

3. The Cross-Spectral Density of the Noise Field

To construct the noise field, we assume that a set of independent, impulsive point sources is Poisson distributed (in time and space) on a large (infinite) spherical shell of radius r', whose centre is coincident with that of the spherical target. Thus, the surface of noise sources is concentric with the surface of the scattering object. A receiver array, consisting of a line of equidistant hydrophones, acting as the acoustic lens, is aligned radially with respect to the target sphere. The phase centre of the array is located at a distance R from the centre of the scattering sphere. The geometry of the source sphere, target sphere and array is shown in Fig. 4.

The acoustic contrast of the scattering sphere is defined as the (intensity) ratio of

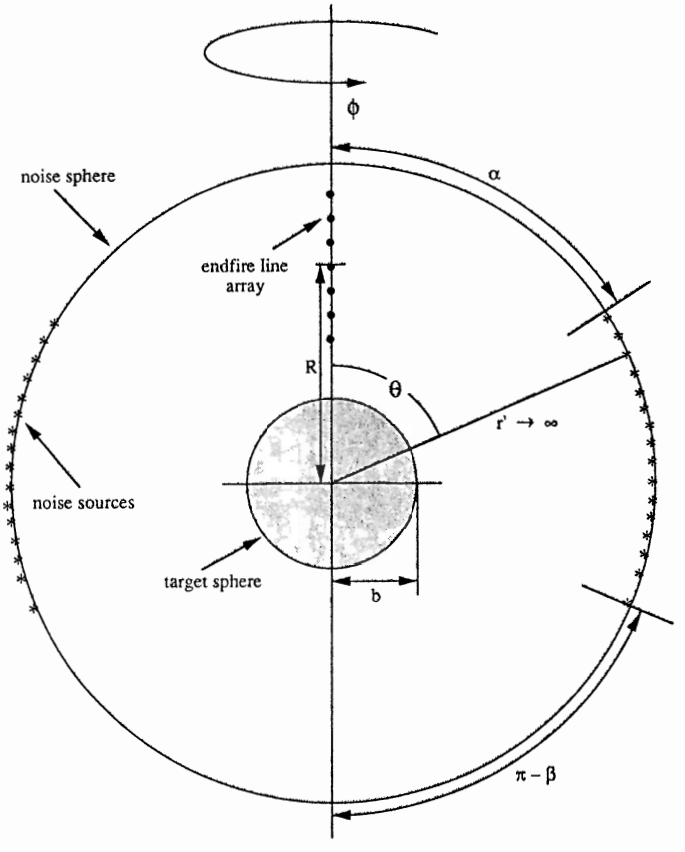

Fig. 4. Configuration of the endfire line array, the target sphere and the large sphere of noise sources used in the analysis of the acoustic contrast of the target in noise fields showing various degrees of anisotropy.

the total (incident plus scattered) noise field to the incident noise field, as observed at the output of the line array. Thus, to determine the acoustic contrast, we need to derive the noise power at the output of the array. In addressing this problem, it is convenient to retain the spherical polar coordinate system of the previous section, with origin at the centre of the scattering object, but with the axis now coincident with the line array. The noise sources are distributed uniformly over a limited area of the source sphere, defined as the surface of revolution lying between the polar angles α and β (Fig. 4). Outside this angular region, the source density is zero. This arrangement of noise sources has the advantage of showing azimuthal uniformity around the line array whilst allowing considerable anisotropy to be introduced into the noise field through the choice of the angles α and β.

The cross-spectrum of the noise field at a pair of sensors, say the pth and qth, in the line array is derived with the aid of Carson's theorem, which concerns random pulse trains. Suppose that a succession of pulses is generated randomly (i.e. the pulses are Poisson distributed in time) by a large number of collocated sources. The resultant time series at either sensor is known as a random pulse train and can be represented by the linear

superposition

$$x_i(t) = \sum_{m=1}^{M} a_m g_i(t - t_m), \quad i = p,\ q, \tag{23}$$

where a_m is the amplitude and t_m is the time of arrival of the mth pulse. The pulse shape functions, $g_i(t)$, are zero, for $t < 0$, to satisfy causality. Although $g_p(t)$ and $g_q(t)$ are not necessarily equal, due to differing propagation paths, there is a one-to-one correspondence between the pulses in each waveform, since the two pulse trains have a common origin. Bearing in mind that the arrival times are Poisson distributed, Carson's theorem states that the cross-spectral density between $x_p(t)$ and $x_q(t)$ is[2]

$$\langle S_{pq}(\omega)\rangle = 2\mu\langle a^2\rangle G_p(j\omega)G_q^*(j\omega), \tag{24}$$

where the symbol $\langle\ \rangle$ indicates an ensemble average, μ is the mean rate of pulses, $\langle a^2\rangle$ is the mean-square pulse amplitude, the asterisk denotes complex conjugation and $G_i(j\omega)$ is the Fourier transform (with respect to time) of the pulse shape function $g_i(t)$, $i = p, q$. In fact, in the context of our ambient noise analysis, it is fairly evident that $G_i(j\omega)$ can be identified with the Green's function derived in the previous section. Equation (24) is an interesting result, not least because it states that a second-order *statistical* quantity, the cross-spectral density, can be expressed entirely (apart from a scaling factor) in terms of the *deterministic* Fourier transforms of the pulse shape functions.

Returning to Fig. 4, consider those sources on the large sphere that occupy an element of surface of area $dA = r'^2 \sin\theta\, d\theta\, d\phi$, where θ and ϕ are, respectively, the polar and azimuthal angular coordinates of dA. The sources localized within dA generate noise waveforms, consisting of a succession of pulses, at the pth and qth receivers in the line array. From Carson's theorem, the cross-spectral density of these random pulse trains is

$$dP_{pq} = 2\chi G_p G_q^* r'^2 \sin\theta\, d\theta\, d\phi, \tag{25}$$

where χ is the mean rate of pulses per unit area, and it is to be understood that P_{pq} is an ensemble average. (The symbol $\langle\ \rangle$ around P_{pq} in Eq. (25) has been omitted for brevity.) If now we allow the radius of the source sphere to be infinitely large, the Green's functions G_p and G_q in this expression, which, from symmetry, are functions of θ but not ϕ, are given by Eq. (10).

On integrating over the entire distribution of sources, we find that the cross-spectral density between the noise fluctuations at the two receivers from all the sources in the angular interval $\alpha \le \theta \le \beta$ on the outer sphere is

$$P_{pq} = \frac{\chi Q^2}{2k\sqrt{r_p r_q}} \int_\alpha^\beta (S_p - T_p)(S_q - T_q)^* \sin\theta\, d\theta, \tag{26}$$

where the subscripts p and q indicate that the associated variable relates to the pth and qth sensor, respectively. For example, r_p is the radial distance to the pth sensor. By multiplying

the two bracketed terms in the integrand, the cross-spectral density in Eq. (26) can be split into the sum of two terms as follows:

$$P_{pq} = P_{pq}^{inc} + P_{pq}^{scat}, \tag{27}$$

where

$$P_{pq}^{inc} = \frac{\chi Q^2}{2k\sqrt{r_p r_q}} \int_{\alpha}^{\beta} S_p S_q^* \sin\theta \, d\theta, \tag{28}$$

and

$$P_{pq}^{scat} = \frac{\chi Q^2}{2k\sqrt{r_p r_q}} \int_{\alpha}^{\beta} (T_p T_q^* - S_p T_q^* - S_q^* T_p) \sin\theta \, d\theta. \tag{29}$$

Thus, P_{pq}^{inc} is the cross-spectral density of the incident field alone. The term P_{pq}^{scat}, on the other hand, consists of three components, one of which is the cross spectrum of the scattered field and the other two are cross-terms representing the coupling between the scattered field and the incident field. Since all three of these terms involve T, the scattered cross-spectral density, P_{pq}^{scat}, is identically zero when $b = 0$.

Equation (26) is a general representation of the cross-spectral density of the total noise field at the pth and qth sensors in the array. Under the limiting condition $kr' \to \infty$, for which Eq. (26) is valid, the incident field consists of a random superposition of plane waves. Since the spatial statistics of plane-wave noise fields are well established,[6] a useful check on Eq. (26) can be performed by examining the spatial coherence of the incident field and comparing the result with the corresponding known coherence functions.

By using the closed form expression in Eq. (11) to represent S, the integral for the cross-spectral density of the incident field in Eq. (28) can be evaluated explicitly, yielding

$$P_{pq}^{inc} = \frac{\chi Q^2}{4\pi} \left[\frac{\exp(-jk\Delta_{pq}\cos\beta) - \exp(-jk\Delta_{pq}\cos\alpha)}{jk\Delta_{pq}} \right], \tag{30}$$

where

$$\Delta_{pq} = r_p - r_q. \tag{31}$$

Now, the spatial coherence of the noise is defined as

$$\Gamma_{pq}^{inc} = \frac{P_{pq}^{inc}}{[P_{pp}^{inc} P_{qq}^{inc}]^{1/2}}, \tag{32}$$

which, when combined with Eq. (30), yields

$$\Gamma_{pq}^{inc} = \frac{\exp(-jk\Delta_{pq}\cos\beta) - \exp(-jk\Delta_{pq}\cos\alpha)}{jk\Delta_{pq}(\cos\alpha - \cos\beta)}. \tag{33}$$

For a uniform distribution of sources over the whole noise sphere (i.e. $\alpha = 0$, $\beta = \pi$), this expression reduces to

$$\Gamma_{pq}^{inc} = \frac{\sin(k\Delta_{pq})}{k\Delta_{pq}}, \tag{34}$$

which is indeed the correct form for the spatial coherence of isotropic, plane-wave noise. Note that this function is real, which is consistent with the symmetry of isotropic noise about the equatorial plane $\theta = \pi/2$; and the zeros occur when the argument of the sine function is a multiple of π, that is to say, when the separation between the two sensors is a multiple of one half-wavelength.

When the sources are uniformly distributed over the hemisphere lying between $\alpha = 0$ and $\beta = \pi/2$, the spatial coherence function in Eq. (33) reduces to

$$\Gamma_{pq}^{inc} = \exp\left[-\frac{jk\Delta_{pq}}{2}\right] \frac{\sin\{k\Delta_{pq}/2\}}{k\Delta_{pq}/2}, \tag{35}$$

which, through lack of symmetry about the equatorial plane, is complex. The zeros in this case occur when the sensor separation is a multiple of one wavelength. If the noise sources were on the opposite hemisphere (i.e. $\alpha = \pi/2$, $\beta = \pi$), then the cross-spectral density would be the conjugate of that in Eq. (35). An independent determination of the noise coherence function, obtained by Fourier transforming the directional density function, shows that Eq. (35) is correct.

On the basis of the results in Eqs. (33) and (34), we conclude that our model of the noise, leading to the formulation of the cross-spectral density in Eq. (26), yields plane-wave noise fields whose spatial and temporal properties are consistent with expectations. With this justification in mind, we proceed below to use Eq. (26) as the fundamental component in our analysis of the acoustic contrast of the target sphere when illuminated by noise sources on the spherical shell of infinite radius.

4. The Contrast Ratio

We shall assume that the linear phased array (Fig. 4), constituting the acoustic lens and consisting of an odd number of unshaded elements at half-wavelength spacing, is steered to endfire. As illustrated in Fig. 5, the beam pattern of such an array shows mirror symmetry about the broadside direction and hence possesses two principal lobes, one in each endfire direction. This simultaneous forward- and backward-looking feature distinguishes the endfire line array from the parabolic reflector used in our original acoustic daylight experiment conducted off Scripps pier, which of course showed only a forward-looking lobe. In certain circumstances, the backward-looking lobe of the line array degrades the acoustic contrast, since it increases the contribution of the incident field to the output power.

The total noise power at the output of an array of $(2N + 1)$ elements, where N is an integer, may be expressed by summing P_{pq} over all values of p and q (taking due account of the endfire steering delays, τ_p and τ_q, applied to the pth and qth sensors):

$$\begin{aligned} P &= \sum_{p,q=-N}^{N} P_{pq} \exp[j\omega(\tau_p - \tau_q)] \\ &= P^{inc} + P^{scat}, \end{aligned} \tag{36}$$

where P^{inc} and P^{scat} are, respectively, the incident and scattered power components at the output of the array. According to the definition given in Sec. 3, the acoustic contrast is

$$C = \frac{P^{inc} + P^{scat}}{P^{inc}} = 1 + \frac{P^{scat}}{P^{inc}}. \tag{37}$$

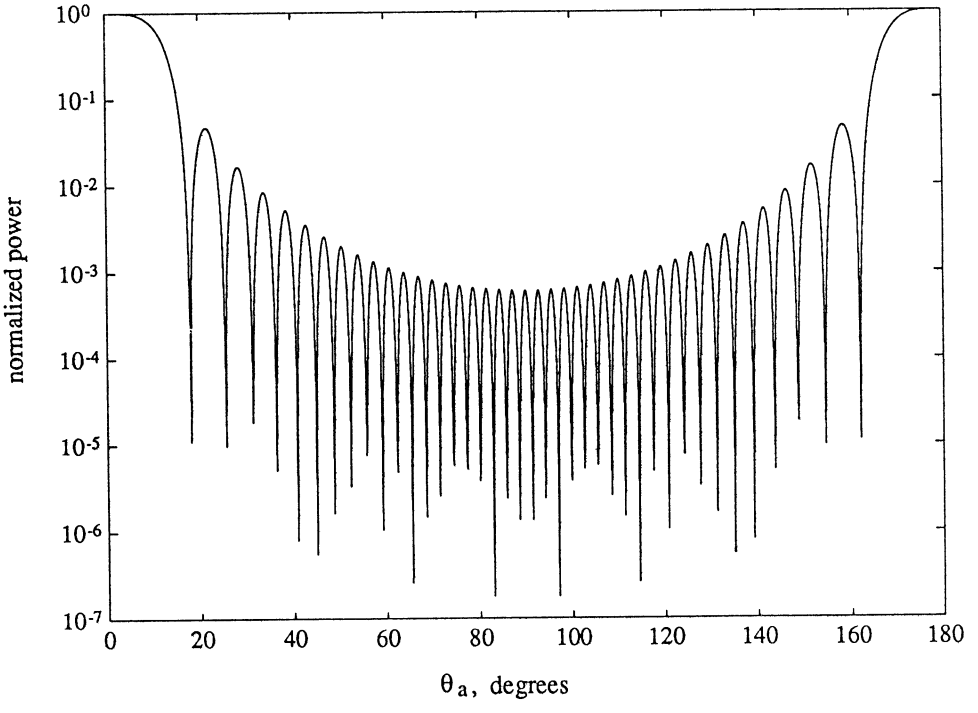

Fig. 5. Beam pattern of an endfire line array of 41 elements at half-wavelength spacing. The arrival angle, θ_a, is measured from the axis of the array. Notice that the beam pattern shows mirror symmetry about the broadside position ($\theta_a = 90°$), with a principal lobe in each endfire direction ($\theta_a = 0°$ and $180°$).

From Eqs. (26)–(29), it follows that

$$P^{inc} = \sum_{p,q=-N}^{N} P_{pq}^{inc} \exp[j\omega(\tau_p - \tau_q)] = \frac{\chi Q^2}{2k} \sum_{p,q=-N}^{N} \frac{\exp[j\omega(\tau_p - \tau_q)]}{\sqrt{r_p r_q}} I_{pq}, \tag{38}$$

and

$$\begin{aligned} P^{scat} &= \sum_{p,q=-N}^{N} P_{pq}^{scat} \exp[j\omega(\tau_p - \tau_q)] \\ &= \frac{\chi Q^2}{2k} \sum_{p,q=-N}^{N} \frac{\exp[j\omega(\tau_p - \tau_q)]}{\sqrt{r_p r_q}} [K_{pq} - (J_{pq} + J_{pq}^*)], \end{aligned} \tag{39}$$

where

$$I_{pq} = \int_{\alpha}^{\beta} S_p S_q^* \sin\theta \, d\theta \,, \tag{40}$$

$$J_{pq} = \int_{\alpha}^{\beta} S_p T_q^* \sin\theta \, d\theta \,, \tag{41}$$

and

$$K_{pq} = \int_{\alpha}^{\beta} T_p T_q^* \sin\theta \, d\theta \,. \tag{42}$$

To evaluate these integrals, we shall use the closed form expressions for S and T in Eqs. (11) and (22), respectively. In fact, the first integral for the incident field is already known from Eq. (30):

$$I_{pq} = \frac{k\sqrt{r_p r_q}}{2\pi}\left[\frac{\exp(-jk\Delta_{pq}\cos\beta) - \exp(-jk\Delta_{pq}\cos\alpha)}{jk\Delta_{pq}}\right] . \tag{43}$$

Some straightforward algebra shows that the second integral is

$$J_{pq} = -\frac{kb}{2\sqrt{2\pi k(r_q - b)}}[\Phi_{pq}(\sqrt{j}u_\beta) - \Phi_{pq}(\sqrt{j}u_\alpha)]$$
$$\times \exp j\left[k\Delta_{pq} + \frac{kb^2\Delta_{pq}^2}{2(r_q - b)r_p r_q} - \frac{\pi}{4}\right] , \tag{44}$$

where $\Phi_{pq}(\sqrt{j}u_x)$ is the following probability integral (which, as Lebedev[9] discusses, is related to the Fresnel integrals):

$$\Phi_{pq}(\sqrt{j}u_x) = 2\sqrt{\frac{j}{\pi}}\int_0^{u_x} \exp(-ju^2)du \,,$$
$$u_x = \sqrt{\frac{kr_p}{2bb'_q}}\left[Z_q(x) - \frac{bb'_q}{r_p}\right] . \tag{45}$$

The function Z_q in this expression is defined in Eq. (20). The third integral is rather more troublesome to evaluate for it can be expressed explicitly only when $p = q$. In this case, an elementary calculation shows that

$$K_{pp} = \frac{kbb'_p}{4\pi r_p}\ln\left\{\frac{(b'_p - b)^2 + 4bb'_p\cos^2(\alpha/2)}{(b'_p - b)^2 + 4bb'_p\cos^2(\beta/2)}\right\} . \tag{46}$$

When $p \neq q$, the integrand in Eq. (42) is highly oscillatory:

$$K_{pq} = \frac{kb^2 b'_p b'_q}{2\pi\sqrt{r_p r_q}}\exp[jk(\Delta_{pq} + b'_p - b'_q)]\int_{\alpha}^{\beta}\sin\theta\frac{\exp[-jk(Z_p - Z_q)]}{Z_p Z_q}d\theta \,. \tag{47}$$

After some algebraic manipulation, the integral here can be converted to a form which is

suitable for evaluation by the standard technique of first-order stationary phase. Appendix A contains the details of the analysis, which leads to the result

$$K_{pq} = \frac{kb^2 b'_p b'_q}{2\pi\sqrt{r_p r_q}} \exp[jk(\Delta_{pq} + b'_p - b'_q)][U_{pq} + E_{pq}], \quad p \neq q, \tag{48}$$

where

$$U_{pq} = \frac{1}{b^2}\sqrt{\frac{2\pi}{kb}} \frac{(r_p - b)(r_q - b)}{(r_p r_q)^{1/4}|r_p - r_q|^{1/2} b^{3/4}(r_p + r_q - b)^{1/4}}$$
$$\times \exp\left[jkb\left\{\frac{(r_p - r_q)(r_p + r_q - b)^{1/2} b^{3/2}}{\sqrt{r_p r_q}(r_p - b)(r_q - b)}\right\} + j\,\mathrm{sgn}(p - q)\frac{\pi}{4}\right] \tag{49}$$

is non-zero when the stationary point lies between the upper and lower limits on the integral, and

$$E_{pq} = \frac{1}{jkb}\left\{\frac{\exp jk[Z_q(\alpha) - Z_p(\alpha)]}{[b'_q Z_p(\alpha) - b'_p Z_q(\alpha)]} - \frac{\exp jk[Z_q(\beta) - Z_p(\beta)]}{[b'_q Z_p(\beta) - b'_p Z_q(\beta)]}\right\} \tag{50}$$

is the endpoint contribution.[7]

The range to the pth element in the array can be written as

$$kr_p = k(R + p\Delta) = kR + p\pi, \tag{51}$$

where R is the range from the centre of the target sphere to the phase centre of the array and Δ, the inter-element spacing, has been equated to one half-wavelength. Following plane-wave beamforming principles (even though the scattered field is not plane-wave), the steering delays in Eqs. (38) and (39) are set to scale with distance from the phase centre:

$$\omega\tau_p = pk\Delta = p\pi. \tag{52}$$

Equation (52) corresponds to the endfire steering condition.

With the above results established, we now have all the ingredients necessary to evaluate the acoustic contrast of the pressure-release sphere. A simplification of the expression for the incident power in Eq. (38) is, however, possible. From the symmetry of the double summation over p and q, it follows that

$$P^{inc} = \frac{\chi Q^2}{2k} \cdot \frac{k}{2\pi} \sum_{p,q=-N}^{N} \left\{\frac{\sin[(p - q)y_\beta] - \sin[(p - q)y_\alpha]}{(p - q)k\Delta}\right\}, \tag{53}$$

where

$$y_x = k\Delta(1 - \cos x). \tag{54}$$

By re-arranging Eq. (53) as a series of (single) summations over fixed values of $(p - q)$, we find that

$$P^{inc} = \frac{\chi Q^2}{2k} \cdot \frac{1}{2\Delta\pi}(S_\beta - S_\alpha), \tag{55}$$

where

$$S_x = \sum_{p,q=-N}^{N} \frac{\sin[(p-q)y_x]}{(p-q)}$$

$$= (2N+1)y_x + 2\left\{2N \sin y_x + \frac{(2N-1)}{2}\sin 2y_x + \frac{(2N-2)}{3}\sin 3y_x + \cdots\right\}$$

$$= (2N+1)y_x + 2\sum_{s=1}^{2N}\frac{(2N-s+1)}{s}\sin sy_x$$

$$= (2N+1)y_x - \frac{\sin[(2N+1)y_x/2]\sin Ny_x}{\sin y_x} + (2N+1)\sum_{s=1}^{2N}\frac{\sin sy_x}{s}. \tag{56}$$

Thus, the expression for the acoustic contrast in Eq. (37) reduces to

$$C = 1 + \frac{2\pi\Delta}{R(S_\beta - S_\alpha)}\sum_{p,q=-N}^{N}\frac{\exp[jk\Delta(p-q)]}{\sqrt{[1+(p\Delta/R)][1+(q\Delta/R)]}}[K_{pq} - (J_{pq} + J_{pq}^*)]. \tag{57}$$

This, our final formulation for C, must be computed numerically using the expressions for the integrals and the sums $S_{\alpha,\beta}$ given above, because no reasonable approximations exist that would allow the double summation in Eq. (57) to be expressed explicitly. (Notice that, through R, the contrast depends on the position of the array relative to the target sphere, which is consistent with the fact that the scattered noise field is spatially inhomogeneous.)

Clearly, when the second term on the right in Eq. (57) is zero, the acoustic contrast is unity, that is to say, the sphere is indistinguishable from the background radiation. Incoherent imaging of the target in this situation would be impossible. Positive contrast, corresponding to frontal illumination, is represented by values of C greater than unity, whereas negative contrast, prevailing when the target is in silhouette, is described by values of C less than unity but greater than zero of course since C is a ratio of acoustic powers. This asymmetry about unity is removed by expressing the acoustic contrast logarithmically. To this end, we define the acoustic visibility, V, as the contrast, C, in dB:

$$V = 10 \log_{10} C. \tag{58}$$

Obviously, negative values of V correspond to negative contrast and positive values to positive contrast.

5. Visibility with a Single Point Sensor

Before considering the full endfire line array, it is instructive to examine the visibility of the target sphere with just a single element of the array. Since an individual sensor is omnidirectional, its response to the incident noise field will be high relative to the response

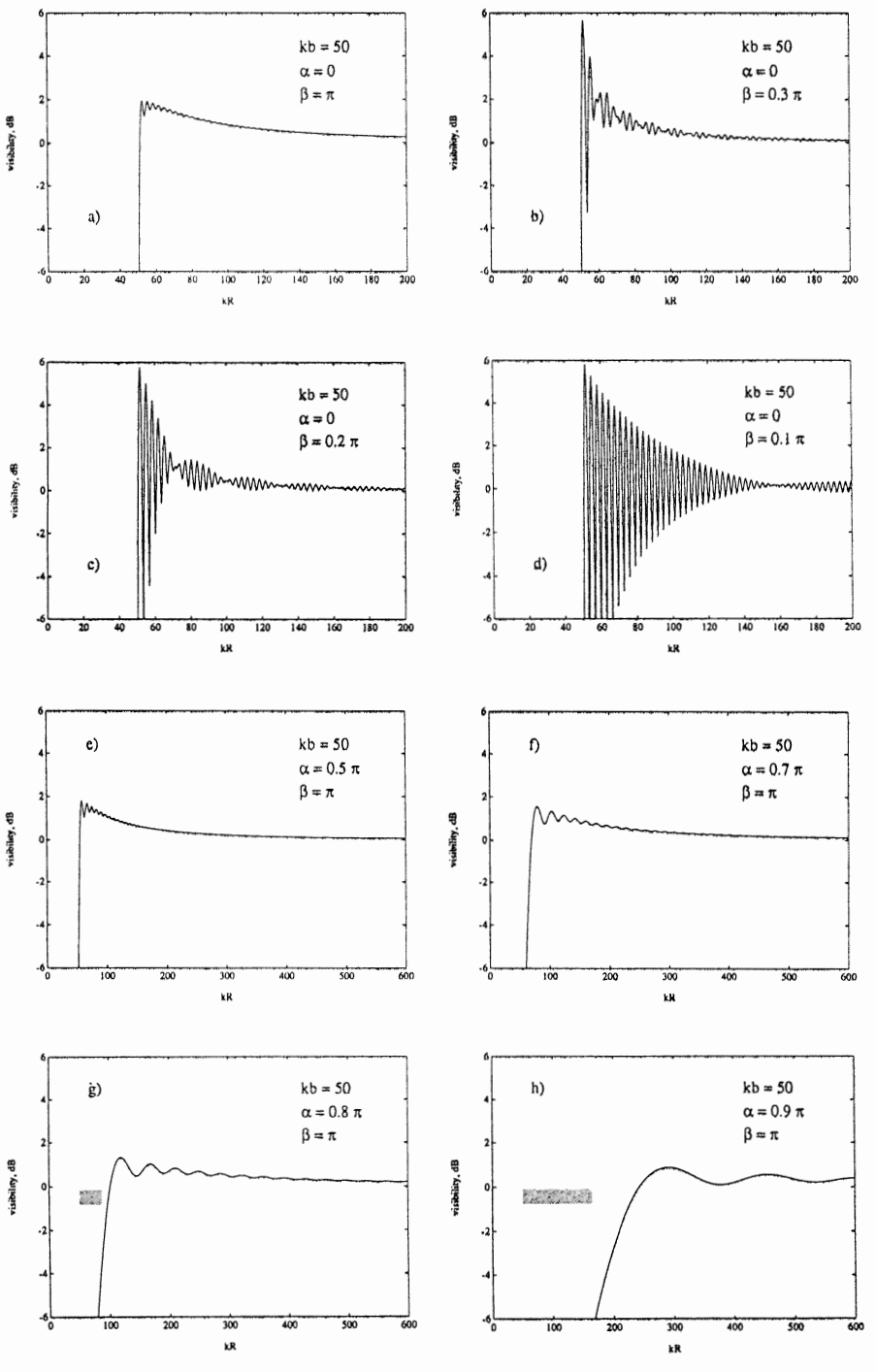

Fig. 6. Visibility of the target sphere with a single point sensor, evaluated from Eqs. (57) and (58) with N set to zero. a) Isotropic noise, b) to d) front-illumination, and e) to h) back-illumination (silhouette). In g) and h), the extent of the umbra is indicated by the stippled horizontal stripe, as calculated from simple geometrical (ray) acoustics.

to the scattered field and, correspondingly, the acoustic visibility will be low. The extended aperture of the full array of sensors overcomes this problem through the formation of a beam whose angular width is comparable with the angle subtended by the target, thus rejecting much of the incident noise whilst retaining most or all of the scattered field. A single sensor should, nevertheless, respond to prominent features in the field, such as the shadow created by the target under back illumination.

Figure 6 shows the visibility from a single sensor as a function of range R (in wavelengths) from the centre of the target sphere, under various degrees of anisotropy in the noise distribution (i.e. for several combinations of α and β). In all cases, the visibility goes to $-\infty$ when $R = b$, as it must to satisfy the pressure-release boundary condition on the sphere. It is interesting that even in isotropic noise (Fig. 6a), with just a point sensor, the target is just visible out to a range of about four sphere radii. Evidently, the boundary condition on the surface of the target sphere forces a modification of the noise field whose effect is easily detectable over a volume some 64 times greater than that of the scattering sphere itself.

The rapid oscillations exhibited by the visibility in isotropic noise (Fig. 6a) and under front-illumination (Figs. 6b, c and d) are due to interference between the incident and scattered fields, an effect which has features in common with the Lloyd's mirror phenomenon, observed when sound from a point source reflects off a plane, pressure-release boundary. As range from the target increases, the amplitude of these oscillations decreases, consistent with the progressively diminishing level of the scattered field.

Under back-illumination conditions (Figs. 6e, f, g and h), the most pronounced feature of the visibility is the region of large negative values, corresponding to the geometrical shadow (umbra) which appears on the side of the target remote from the noise sources. The extent of the umbra is delineated explicitly in Figs. 6g and h. At ranges beyond the umbra, the visibility shows slow oscillations (compared to the rapidly varying Lloyd's mirror-type fringes observed under front-illumination) which arise from diffraction around the scattering sphere. Even under front-illumination, there is some evidence of diffraction in the form of a slow modulation of the rapid interference oscillations (see e.g. Fig. 6c).

It is evident from Fig. 6 that, when an omnidirectional point sensor constitutes the "acoustic lens", the degree of anisotropy in the noise is not a critical factor in determining the visibility of the target. With front-, back-, or isotropic illumination, the target is visible (positive or negative) out to ranges of several target-sphere radii. This relative insensitivity to the directionality of the noise indicates a degree of robustness that is highly desirable in connection with the acoustic daylight technique of incoherent imaging.

6. Visibility with a Full Endfire Line Array

Although the sphere is detectable with a point sensor, it is clear that the magnitude of the visibility can be significantly improved by using an acoustic lens showing a strong directional response. This is illustrated in Fig. 7, which shows the visibility of the target sphere as

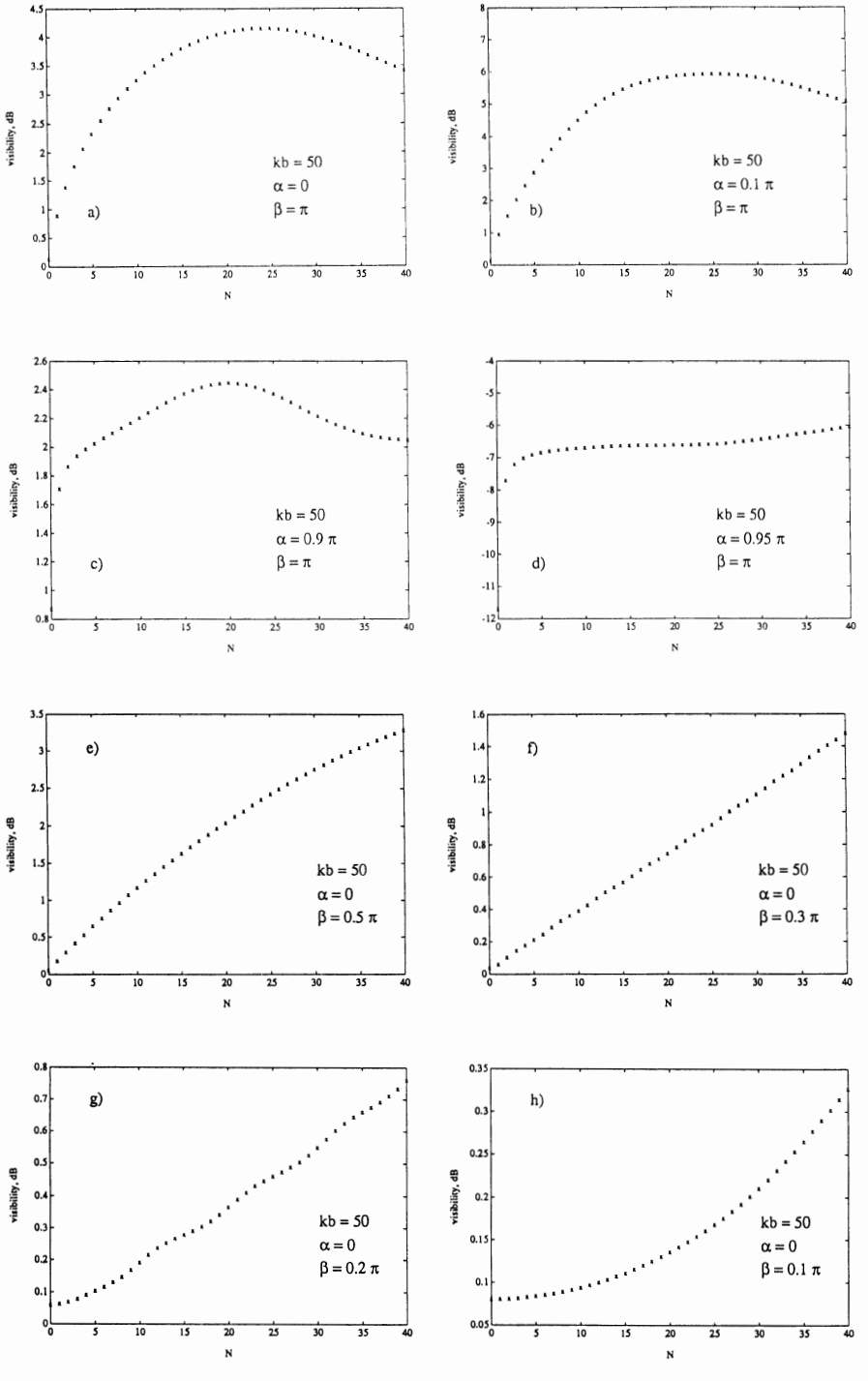

Fig. 7. Visibility of the target sphere with an endfire array of $(2N+1)$ elements at half-wavelength spacing, as calculated from Eqs. (57) and (58). a) Isotropic noise, b) to d) back-illuminiation, and e) to h) front-illumination. In all cases, $kR = 400$, where R is the distance from the phase centre of the array to the centre of the target sphere.

a function of the aperture of the endfire line array (Fig. 4) under various conditions of anisotropy in the noise.

In isotropic noise (Fig. 7a), the visibility is positive for all N and shows a broad maximum around $N = 25$, corresponding to a beamwidth between the -3 dB points of 21°. The angle subtended by the target at the phase centre of the array is 19.2°, that is, approximately equal to the beamwidth, indicating that the maximum visibility occurs when the target fully occupies the beam. When the beam is significantly narrower than the angular width of the target, the visibility decreases below the maximum because scattered energy from the sphere is rejected by the array. With a broader beam, on the other hand, more noise is accepted by the array and again the visibility is reduced below the maximum possible level. Thus, it is clear how the beamwidth of the acoustic lens would determine the angular resolution of an acoustic daylight imaging system.

Figure 7b shows the visibility of the target sphere when a "hole" is created in the distribution of noise sources immediately behind the array. The visibility is noticeably enhanced (cf. Fig. 7a), by about 2 dB at the maximum, because of the reduced noise in the backward-looking beam. Under stronger back-illumination, the visibility becomes more uniform with increasing aperture (Fig. 7c), although still remaining positive, but, as the array is plunged into shadow, the visibility goes negative (Fig. 7d), taking values that are hardly dependent on N (since none of the sensors is illuminated).

When the target sphere is observed under frontal illumination with an array of moderate aperture, the visibility increases monotonically as a function of N (Figs. 7e to h). In this situation, most of the scattered energy is concentrated into a solid angle that is narrower than the angular width of the target itself. Thus, although the beam may be considerably narrower than the target, there is no rejection of scattered radiation and no associated decrease in the visibility. This advantage is offset in the case of the endfire array by the fact that the backward-looking beam is directed at a large number of noise sources, which reduces the visibility of the target to unnecessarily low levels. In a practical acoustic lens, the rearward pointing beam would be absent and the visibility under front illumination would be better than is indicated by the plots in Figs. 7e to h.

It is evident from Fig. 7 that the extended aperture formed by the array of hydrophones enhances the visibility of the target to levels which are adequate for performing incoherent imaging. As with the single sensor, the magnitude of the visibility as observed by the array is not critically sensitive to the detailed structure of the noise field, suggesting that, with an appropriate acoustic lens, the acoustic daylight technique could be made to operate successfully in most realistic ambient noise environments.

7. Concluding Remarks

The fact that objects illuminated by ambient light in the atmosphere are optically visible is so familiar that it is usually given little consideration. Yet the physical (and for that matter the physiological) mechanisms by which we are able to see are subtle and interesting: a random optical field is strongly modified by the presence of an object within the field,

through reflection or scattering. The scattered radiation propagates to a receiver, which may be a human eye, and from the contrast between the scattered and background field, the object is perceived. An analogous process of acoustic "vision", involving the ambient noise field in the ocean, is comparatively unfamiliar since it has received little attention in the scientific literature or indeed elsewhere.

The analysis presented in this article concerns the acoustic visibility of an object, a pressure-release sphere, which is illuminated by ambient noise showing various degrees of anisotropy. According to the theory, the sphere scatters the noise field sufficiently to be detectable with a single, omnidirectional hydrophone out to a distance of approximately four sphere radii. The visibility of the sphere with the point sensor is, however, rather poor since there is no rejection of the unwanted incident field. A significant improvement is achieved when the single sensor is replaced with a phased array of hydrophones. Even in isotropic noise, the visibility then shows a peak value of approximately 4 dB, which occurs when the beamwidth of the array matches the angle subtended by the target at the phase centre of the array. This conclusion, derived from theoretical considerations, is quantitatively consistent with the results of the acoustic daylight experiments conducted recently off Scripps pier.[5]

Acknowledgment

The research reported in this paper was supported by the US Office of Naval Research under contract N00014-91-J-1118.

Appendix A. Evaluation of the Integral K_{pq} by First-Order Stationary Phase

The integral to be evaluated in Eq. (47) is

$$K_{pq} = \int_{\alpha}^{\beta} \sin\theta \frac{\exp[-jk(Z_p - Z_q)]}{Z_p Z_q} d\theta , \tag{A.1}$$

where

$$Z_p = b\sqrt{f_p + g_p \cos^2(\theta/2)} , \tag{A.2}$$

$$f_p = \frac{b^2}{(r_p - b)^2} , \tag{A.3}$$

and

$$g_p = \frac{4r_p}{(r_p - b)} . \tag{A.4}$$

Now, the phase term $(Z_p - Z_q)$ in the integrand of Eq. (A.1) has no turning point and hence the integral cannot be evaluated by the method of stationary phase as it stands. However,

by making the substitution

$$s^2 = f_p + g_p \cos^2(\theta/2), \tag{A.5}$$

the integral becomes

$$K_{pq} = -\frac{4}{b^2 g_p} \int_{s_\alpha}^{s_\beta} \frac{\exp[-jkb\{s - \sqrt{f_p + (g_q/g_p)(s^2 - f_p)}\}]}{\sqrt{f_p + (g_q/g_p)(s^2 - f_p)}} ds, \tag{A.6}$$

where $s_{\alpha,\beta}$ are given by Eq. (A.5) with $\theta = \alpha, \beta$. The new phase term does show a real stationary point, thus allowing a stationary phase analysis to be applied.

Since the exponent in Eq. (A.6) is

$$y = \sqrt{f_p + (g_q/g_p)(s^2 - f_p)} - s, \tag{A.7}$$

the first and second derivatives of the phase are, respectively,

$$y' = \frac{ws}{\sqrt{ws^2 + a}} - 1, \tag{A.8}$$

and

$$y'' = \frac{wa}{(ws^2 + a)^{3/2}}, \tag{A.9}$$

where

$$w = \frac{g_q}{g_p} \quad \text{and} \quad a = f_q - w f_p. \tag{A.10}$$

By equating Eq. (A.8) to zero, the stationary point is found to be

$$s_0 = \sqrt{\frac{a}{w(w-1)}}, \tag{A.11}$$

provided $w > 1$, or equivalently, $r_p > r_q$. (If this condition is not satisfied, then the subscripts on the right in Eq. (A.5) should be q rather than p.) The second derivative at the turning point is

$$y''|_{s=s_0} = \frac{(w-1)^{3/2}}{(wa)^{1/2}} > 0. \tag{A.12}$$

From standard first-order stationary phase theory, the contribution to the integral K_{pq} from around the turning point is

$$U_{pq} = \frac{1}{b^2}\sqrt{\frac{2\pi}{kb}} \frac{(r_p - b)(r_q - b)}{(r_p r_q)^{1/4}|r_p - r_q|^{1/2} b^{3/4}(r_p + r_q - b)^{1/4}}$$
$$\times \exp\left[jkb\left\{\frac{(r_p - r_q)(r_p + r_q - b)^{1/2} b^{3/2}}{\sqrt{r_p r_q}(r_p - b)(r_q - b)}\right\} + j\,\mathrm{sgn}(p - q)\frac{\pi}{4}\right], \tag{A.13}$$

which is valid for all p and q. The endpoint contributions to the integral in Eq. (A.6) are obtained by a routine partial integration, but retaining only the integrated parts:

$$E_{pq} = \frac{1}{jkb}\left\{\frac{\exp\, jk[Z_q(\alpha) - Z_p(\alpha)]}{[b'_q Z_p(\alpha) - b'_p Z_q(\alpha)]} - \frac{\exp\, jk[Z_q(\beta) - Z_p(\beta)]}{[b'_q Z_p(\beta) - b'_p Z_q(\beta)]}\right\}. \tag{A.14}$$

The integral K_{pq} is just the sum of the contributions from the turning point and the endpoints:

$$K_{pq} \approx U_{pq} + E_{pq}\,, \tag{A.15}$$

which is the result cited in Eqs. (48) to (50) of the main text.

References

1. G. Arfken, *Mathematical Methods for Physicists*, 3rd ed. (Academic Press, San Diego, 1985) p. 618.
2. M. J. Buckingham, *Noise in Electronic Devices and Systems* (Ellis Horwood, Chichester, 1983).
3. M. J. Buckingham, Personal Communication to Dr. David Bradley, Naval Research Laboratory, Washington DC, 1987.
4. M. J. Buckingham, "Spherically symmetrical acoustic propagation across a fluid/fluid boundary", *J. Acoust. Soc. Am.* **83** (1988) 566–570.
5. M. J. Buckingham, B. V. Berkhout and S. A. L. Glegg, "Imaging the ocean with ambient noise", *Nature* **356** (26 March 1992) 327–329.
6. H. Cox, "Spatial correlation in arbitrary noise fields with application to ambient sea noise", *J. Acoust. Soc. Am.* **54** (1973) 1289–1301.
7. L. B. Felsen and N. Marcuvitz, *Radiation and Scattering of Waves* (Prentice-Hall, Englewood Cliffs, NJ, 1973) pp. 386–391.
8. N. N. Lebedev, *Special Functions and their Applications* (Prentice-Hall, Englewood Cliffs, NJ, 1965) p. 126.
9. N. N. Lebedev, *Special Functions and their Applications* (Prentice-Hall, Englewood Cliffs, NJ, 1965) pp. 21–23.
10. P. M. Morse and H. Feshbach, *Methods of Theoretical Physics* (McGraw-Hill, NY, 1953) pp. 1483–1486.
11. P. M. Morse and K. U. Ingard, *Theoretical Acoustics* (McGraw-Hill, NY, 1968) p. 419.
12. V. A. Shchurov, "Coherent and diffusive fields of underwater acoustic ambient noise", *J. Acoust. Soc. Am.* **90** (1991) 991–1001
13. G. N. Watson, *A Treatise on the Theory of Bessel Functions* (Cambridge Univ. Press, 1958) p. 368.